Research in Astron. Astrophys. **2009** Vol. **9** No. **3**, 367–376
http://www.raa-journal.org *http://www.iop.org/journals/raa*

***R**esearch in*
***A**stronomy and*
***A**strophysics*

Measurements of electronic properties of the Miyun 50 m Radio Telescope

Xi-Zhen Zhang, Xin-Ying Zhu, De-Qing Kong, Lei Zheng, Cheng Yao, Hong-Bo Zhang, Yan Su and Ting-Yi Piao

National Astronomical Observatories, Chinese Academy of Sciences, Beijing 100012, China; *zxz@bao.ac.cn*

Received 2008 March 19; accepted 2008 August 15

Abstract Measurement results of some properties of the Miyun 50 m radio telescope (MRT50) of the National Astronomical Observatories, such as pointing calibration, antenna beams, system noise temperature, gain and gain variations with elevation are introduced. By using a new de-convolution technique developed by our group, the broadening effect on measured beams caused by the width of an extended radio source has been removed so that we obtained higher accuracy on the measurements of MRT50 beams.

Key words: instrument: telescope — antenna — method

1 INTRODUCTION

In 1999, after the Miyun Synthesis Radio Telescope (MSRT) finished its main scientific goal: the meter-wave radio source survey (Zhang et al. 1997), Miyun radio group proposed to build a 45 m single dish telescope (Zhang et al. 2000) for radio astronomy research at low frequency bands. Afterwards, it was suggested that the project construct a more multi-function 50 m radio telescope for both radio astronomical observations and space communications in 2002 (Wang 2002). The MRT50 was put into test operation in 2005 and passed its final reception test in 2006. Section 2 gives a short introduction to the MRT50.

In general, some necessary tests, such as pointing calibration, beam-size/efficiency determination, gain measurements, and so on, have to be done before the telescope can be used correctly. First of all, pointing calibration was carried out during the test period of MRT50 in 2005. The pointing accuracy reached about 30″ after the first calibration. This made the observation of SMART-1 successful in the summer of 2005. The second round of pointing calibration was continued in 2006 (after Meeks et al. 1968; Yuan et al. 1986). We will introduce the pointing calibration method and result in Section 3.

To determine antenna gain with a cosmic source, it is expected that the source is small in angular size and strong in intensity. If a large angular source is used, the measured beam width has to be corrected (Yuan et al. 1986). Because of the sensitivity of MRT50, the radio source Cyg A was adopted to determine the beams. To reduce the effect of Cyg A structure, a new de-convolution method, developed by our group, was used to remove the broadening effect. The de-convolution method, results of antenna gain and gain variations with antenna elevation will be introduced in Section 4. Related observations were performed in 2007. In Section 5, we will give the results of equivalent noise temperature at the input-port of LNA and its variations with antenna elevation.

2 MIYUN 50 M RADIO TELESCOPE

The MRT50 is located at the Miyun Station of the National Astronomical Observatories, with longitude 116.976 E, latitude 40.558 N, and elevation 155 m (see Fig. 1).

Fig. 1 The Miyun 50 m Radio Telescope.

The Miyun Radio Telescope (MRT50), which is 50 meters in diameter, is a wheel-on-track system with an Azimuth-Elevation frame structure. It consists of a parabolic reflector, which is made from a solid filled panel in the inner 30 m region and wire mesh in the outer 30 m region, and some multi-function receiver back-ends. The antenna has primary feeds working at UHF1/UHF2, L, S/X and Ku bands. The feed selected can be rotated to the right position automatically to change the observing frequency and moved along the reflector axis. Both the rotation and movement of the selected feed can compensate the variation of the reflector focus caused by gravitation. Tables 1 and 2 list the mechanical and electronic properties of the antenna respectively (measured by the antenna maker, the $54^{\rm th}$ institute of CETC, in 2006).

Table 1 Main Mechanical Specifications of the Miyun 50 m Antenna

Items	Azimuth	Elevation
Movable range	$\pm 270^\circ$	$+5^\circ \sim +90^\circ$
Maximum slewing speed (deg s^{-1})	1.0	0.5
Slewing speed while accurately controlling (deg s^{-1})	$0.003^\circ \sim 0.3^\circ$	$0.0015^\circ \sim 0.15^\circ$
Maximum acceleration (deg s^{-2})	0.5	0.3
Acceleration while accurately controlling (deg s^{-2})	0.015	0.015
Surface rms ($<$ 30m)	0.75 mm	
Surface rms (30–50m)	1.06 mm	
Optics	Prime focus, F/D=0.35	
Maximum wind speed while accurately controlling	17 m s^{-1}	

By making use of the UHF1/UHF2 and S/X frequency groups, a design of interplanetary scintillation (IPS) monitoring system has been performed recently (Zhang 2007). An L-band pulsar receiver is now under construction for the MRT50 (Jin et al. 2006). The MRT50 is one of the key-sites for downloading scientific data from the CE-1 lunar satellite and taking part in measurements of its orbit.

3 POINTING CALIBRATION OF THE MRT50

In general, a new large aperture radio telescope ($D > 100\lambda$) cannot point at a radio source using the coder only because there are a lot of system errors such as axial error, basic plane error, and so on.

Table 2 Main Electronic Specifications of the Miyun 50m Antenna

Tracking mode	Programming, Automatic
Pointing accuracy	19″ (r.m.s)
Frequency/band width (MHz)	327/30,611/60,1650/330,2300/460, 8400/1600,12100/800
VSWR	$\leq$1.3 (single feed), $\leq$1.5 (dual-frequency feed)
First side-lobe(dB)	$\leq$–18
Cross couple between two polarization channel (dB)	$\leq$–20
Cross couple between different frequency channel (dB)	$<$–20
Antenna temperature at feed output point	$<$17 K for all bands
Antenna efficiency	57.3%@345 (MHz) 57.0%@611 (MHz) 60.2%@1537 (MHz) 59.9%@2500 (MHz) 68.4%@7600 (MHz)(43 m diameter) 62.9%@12250 (MHz)(33 m diameter)

Table 3 Information of the Pointing Calibration Sources for MRT50

Source name	R.A.(2000)	Dec.(2000)	Type/size(″)	Flux(Jy)X band
3C 48	01 37 41.27	33 09 35.7	QSO /$<$1.5	3.5
3C 84	03 19 48.16	41 30 42.1	Gal./$<$1.0	40.0
3C 123	04 37 04.17	29 40 15.1	Gal./23	12.0
3C 144	05 34 32.	22 00 58.	SNR /180 $\times$ 240	560
3C 147	05 42 36.14	49 51 07.2	QSO /$<$1.0	6.0
3C 161	06 27 10.10	–05 53 04.8	Gal./3	4.5
3C 218	09 18 05.70	–12 05 44.0	Gal./$<$ 47 $\times$ 47	9.0
3C 273B	12 29 06.70	02 03 08.60	QSO/$<$20	40.0
3C 274	12 30 49.42	12 23 28.0	Gal./150 $\times$ 250	55.0
3C 279	12 56 11.17	–05 47 21.5	QSO/$<$2.0	13.0
3C 286	13 31 08.29	30 30 33.0	QSO/$<$2.0	6.0
3C 295	14 11 20.65	52 12 09.1	Gal./5 $\times$ 1	4.5
3C 348	16 51 08.20	04 59 33.0	Gal./170.	9.0
3C 353	17 20 28.20	–0058 48.0	Gal./240 $\times$ 240	18.0
3C 380	18 29 31.72	48 44 47.0	QSO/$<$1.0	5.0
3C 405	19 59 28.4	40 44 02.	Gal./170 $\times$ 45	190
3C 461	23 23 24.8	58 48 59.0	SNR/240 $\times$ 240	610
DR 21	05 55 30.81	39 48 49.2	QSO/$<$20	20

So, carrying out system pointing calibration is the first step to use the telescope. There are a number of pioneers who introduced the principle and method to calibrate pointing of a telescope (Meeks et al. 1968; Yuan et al. 1986; Himwich 1993; Iesber 1967; Ulich 1981, 1982). Instead of the fitting method of least squares, which is widely adopted in model fitting of pointing calibration, Kong (2008) introduced a new fitting method, which is named the Generalized Extended Interpolation Correction Method. Zhang (2007) also proposed another model fitting method, named the Least Squares Support Vector Machines (LSSVM). The beam-width of MRT50 at X band is about 200″, which is the highest frequency available so far. The expected pointing calibration accuracy is about 20″.

Sources for calibration observation should have small angular diameter, strong intensity and uniform distribution in the sky. Table 3 lists the sources we used. Some sources with small angular size but are somewhat weak were excluded from this calibration because of the MRT50 sensitivity, whereas some strong and extended sources, for example Cyg A, Cas A, Tau A and Vir A, were used in the first round of observations. Each source was observed at different positions in the sky. In total, 152 positions, which have an almost uniform distribution in the sky, were observed in 2006. Figure 2 gives the distribution of the 152 positions in the sky.

The observations were carried out using two dimensional scans. The measurement values at each position are defined as $\Delta A = A_{\rm obs.} - A_{\rm cal.}$ and $\Delta E = E_{\rm obs.} - E_{\rm cal.}$. Here A is the antenna azimuth and

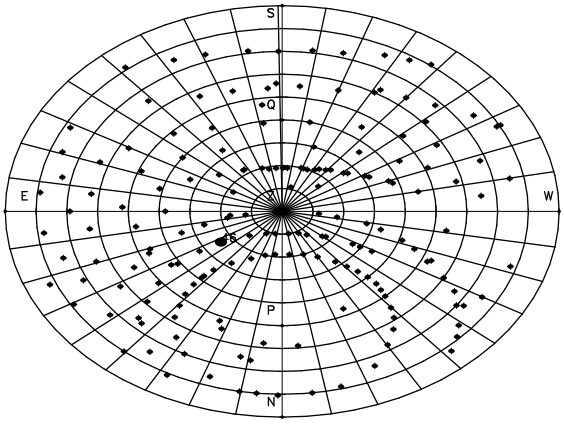

Fig. 2 The sky coverage of the pointing calibration observations.

Table 4 Parameter Values Fitted from the 152 Observational Data (unit is degree for all parameters)

KA	ϕ	κ	ϵ	δ	KH	ato	β
–0.37358	0.01081	–16.75	–0.00308	0.06442	0.028468	0.00208	–0.03919

E is its elevation. To increase the measurement accuracy of ΔA and ΔE, we use a pair of scan-curve median points (Half Maximum Width) to measure $A_{\rm obs.}$ and $E_{\rm obs.}$. This method can reduce the errors because of the different grades near the peak and median points.

The pointing calibration models for MRT50 were built as Equations (1) and (2) (refer to Meeks et al. 1968) from the 152 observations.

$$\Delta A = a_1 \cdot x_1 + a_2 \cdot x_2 + a_3 \cdot x_3 + a_4 \cdot x_4 + a_5 \cdot x_5, \tag{1}$$

$$\Delta E = b_1 \cdot y_1 + b_2 \cdot y_2 + b_3 \cdot y_3 + b_4 \cdot y_4 + b_5 \cdot y_5, \tag{2}$$

where $a_1 = \tan(E) \times \cos(A)$, $a_2 = \tan(E) \times \sin(A)$, $a_3 = \tan(E)$, $a_4 = -\sec(E)$, $a_5 = 1$; $x_1 = -\phi \times \cos(\kappa)$, $x_2 = -\phi \times \sin(\kappa)$, $x_3 = \epsilon$, $x_4 = \delta$, x_5 =KA; $b_1 = -\sin(A)$, $b_2 = \cos(A)$, $b_3 = \cos(E)$, $b_4 = 1/\tan(E)$, $b_5 = 1$; $y_1 = -\phi \times \cos(\kappa)$, $y_2 = -\phi \times \sin(\kappa)$, $y_3 = \beta$, y_4=ato, y_5 =KH.

The parameters used in (1)/(2) are defined as the followings. They are: ϕ – azimuth-axis tilt, $(90^\circ - \kappa)$ – the azimuth toward which the azimuth axis is tilted, $(90^\circ - \epsilon)$ – the elongation between azimuth-axis and the elevation-axis, δ – the collimation error (the axis of the antenna beam is not exactly perpendicular to the elevation axis), KA – constant (the azimuth-axis coding zero-error), β – gravitational deflection error, 'ato' – the residue after calibration of the atmospheric model, KH – constant (the elevation-axis coding zero-error). The parameter values obtained are given in Table 4. Figures 3 and 4 show the distribution of MRT50 pointing residual errors, and the models applied respectively. Our results show that the pointing calibration accuracy (13.5″ in azimuth, 17.5″ in elevation) reached 1/10 beam-width.

For further pointing calibration, using the Ku band may be a good choice. The beam at Ku band of the MRT50 is about 150″ which makes the reachable accuracy of about 15″. In addition, the MRT50 antenna maker, the $54^{\rm th}$ institute of CETC, measured an epsilon value using a mechanical method. The value they found was 12″ while our value is about 11″.

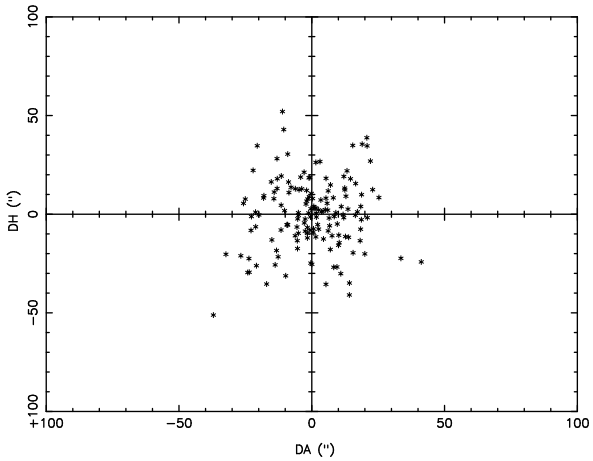

Fig. 3 Distribution of the pointing calibration residues.

4 MEASUREMENTS OF THE MAIN BEAM AND GAIN OF THE MRT50

Ideal radio sources for beam measurement of a radio telescope should be small and strong. However these kinds of sources cannot be used to measure a side-lobe as low as –20 dB for MRT50 because of its sensitivity limitation. The observed beam will be broadened if an extended source is used to measure the beam. Cyg A is a strong radio source with two-point components. It is possible to deal with Cyg A as two small angular sources because of its special structure.

We developed a program to fit the observed scan curve with a calculated curve which convolutes an adjustable beam with a two-point model of Cyg A. The model of Cyg A is defined as the following: two point sources, each is $30''$ in diameter, and the angular spacing between the two points varies with the azimuth and elevation (see Table 5). When the residue between the observed curve and calculated one is small enough, the adjustable beam should be the beam which has no broadening effect on the two-point structure. Figure 5 gives examples at S/X bands. It shows that the residue is smaller than 1% and the fit between the observed curve and the calculated one is quite good. The fit suggests that the beam shape of the MRT50 at X band can be well represented by a Gaussian function. The feed of the S/X band is a compound one. The X band feed is in the center part surrounded by the S band feed. Hence, the beam shape of S band cannot be represented very well by a Gaussian function. It is represented by a modulated Gaussian function. In this case, the residue is also small enough.

4.1 Two Dimensional Main Beam

By using the method described above, we determined the two dimensional MRT50 beams at S/X bands. Cyg A was used as the emitting source. Scans were carried out in the azimuth direction with the intervals of $120''$ at S band and $60''$ at X band in the elevation direction.

Figure 6 shows the measured S and X band beams, which are both symmetric. The beam-width of 3 dB and 10 dB at S band is $11.816'(A)\times11.779'(E)$ and $19.945'(A)\times19.912'(E)$ at elevation 30° respectively, while at X band it is about $3.527'(A)\times3.187'(E)$ and $6.430'(A)\times5.810'(E)$, respectively. The corresponding S/X band gains are 58.8 dB and 69.4 dB, respectively. Our measurements were carried out at 2300 MHz (S band) and 8400 MHz (X band). The MRT50 antenna maker, the CTI $54^{\rm th}$ institute, measured one-dimensional scans using a satellite signal as the emitting source in the azimuth and altitude planes at 2500 MHz and 7600 MHz (not our S/X working frequency) respectively. The MRT50 gains at 2500/7600 MHz were 59.85 dB and 68.37 dB respectively. After changing our gain values to the 2500/7600 MHz, we got 59.52 dB and 68.21 dB. We found that our gain value at X band agrees with their result well while the gains at S band have a 0.33 dB difference. According to the measured

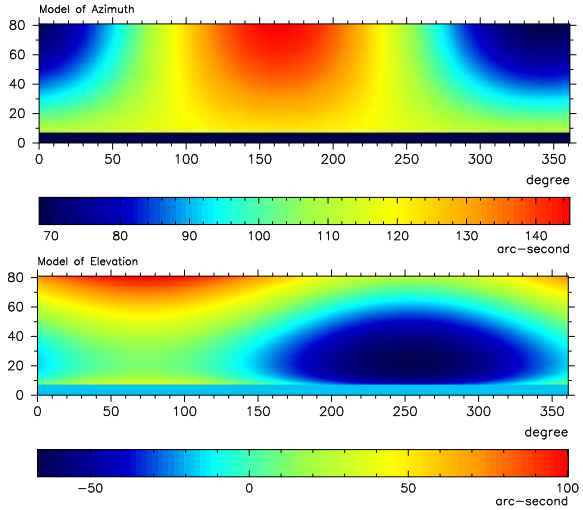

Fig. 4 The azimuth model (top) and the elevation model (bottom) used for the pointing correction of MRT50. The constant term of the model is not displayed in this figure.

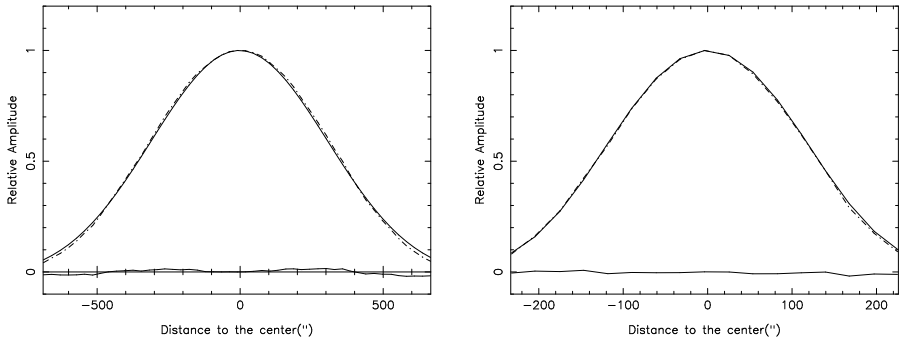

Fig. 5 An example of the de-convolution fit at S band (left) and X band (right), continuous line (up) is the observed curve and the dashed line (up) is the calculated curve, and the lower line is the residue.

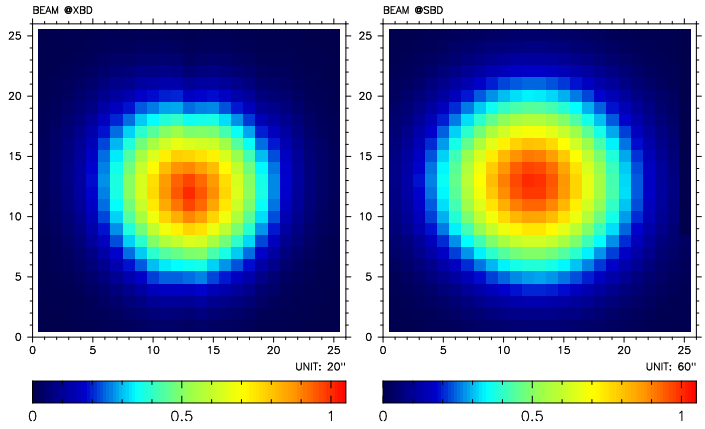

Fig. 6 Main beam of MRT50 at X band (left) and S band (right).

Table 5 Distances between the two-components of the Cyg A in the western and eastern parts of the sky ($da = (a_1 - a_2) \times \cos(h)$, $dh = h_1 - h_2$), where a is the azimuth and h is the elevation in degrees.

West	$a_1(^\circ)$	$a_2(^\circ)$	$h_1(^\circ)$	$h_2(^\circ)$	$da(')$	$dh(')$
	275.0571	274.9711	80.9007	80.9317	0.8160	–1.8640
	275.5492	275.4730	79.3877	79.4185	0.8424	–1.8521
	276.0838	276.0150	77.8760	77.9067	0.8676	–1.8402
	276.6475	276.5844	76.3659	76.3964	0.8913	–1.8292
	—	—	—	—	—	—
	311.9667	311.9357	14.2684	14.2840	1.8047	–0.9369
	313.0168	312.9857	13.1479	13.1630	1.8223	–0.9036
	314.0834	314.0520	12.0466	12.0611	1.8409	–0.8692
	315.1666	315.1351	10.9652	10.9791	1.8569	–0.8340
	316.2668	316.2351	9.9042	9.9175	1.8705	–0.7979
East	$a_1(^\circ)$	$a_2(^\circ)$	$h_1(^\circ)$	$h_2(^\circ)$	$da(')$	$dh(')$
	43.7332	43.7185	9.9042	9.8736	0.8699	1.8388
	44.8334	44.8192	10.9652	10.9342	0.8348	1.8556
	45.9166	45.9030	12.0466	12.0154	0.7993	1.8712
	46.9831	46.9701	13.1479	13.1165	0.7640	1.8856
	48.0333	48.0207	14.2684	14.2367	0.7289	1.8994
	—	—	—	—	—	—
	82.7677	82.8011	74.8575	74.8247	–0.5226	1.9666
	83.3525	83.3913	76.3659	76.3332	–0.5476	1.9597
	83.9162	83.9617	77.8760	77.8435	–0.5733	1.9524
	84.4508	84.5050	79.3877	79.3553	–0.5995	1.9441
	84.9429	85.0089	80.9007	80.8684	–0.6268	1.9359

Table 6 Calculated Parameter Values of the MRT50 Antenna

Term	S band (2300 MHz)	X band (8400 MHz)
$\eta_{\rm ANT}$	92%	88%
$\Omega_{\rm M}$	1.3341×10^{-5}	1.07747×10^{-6}
$\Omega_{\rm A}$	1.52685×10^{-5}	1.27086×10^{-6}
D_0	59.154 dB	69.951 dB
$\eta_{\rm MB}$	87.4%	84.8%
$A_{\rm E}$	1107 $\rm m^2$	1020 $\rm m^2$
$\eta_{\rm AP}$	56.4%	52%

Explanation can be found in Section 4.1

two-dimensional beams, the main beam efficiencies, effective receiving areas, aperture efficiencies, and other parameters at the S/X bands were calculated. Table 6 lists the values. The meanings of the parameters in Table 6 should be clear without any explanation except for the $\eta_{\rm ANT}$ parameter. It is the efficiency of the antenna related to the loss of the reflector shape-errors and the feed (Stutzman 1998). Although the illuminating intensity at the reflector edge (50 m) is about –10 dB and –16 dB for S/X bands respectively, we take the whole reflector area to calculate the aperture efficiencies for both S and X bands (see Table 6). On the other hand, the effective receiving areas we measured come from the radiating property of the whole reflector (50 m), so the whole reflector area should be taken to calculate the aperture efficiencies. This is different from what the $54^{\rm th}$ institute calculated. The illuminating diameter they used at X band is 43 m so that they achieved a higher aperture efficiency number at X band.

4.2 Gain and Gain Variation with Elevation of MRT50

The gain of an antenna may vary with its elevation because gravitation may cause its reflector's shape to change. To measure this property, we measured the gains from 10° – 80° elevation of MRT50. Two scans in the azimuth and elevation planes were recorded with an interval of 5° from 10° – 80°. These two scan data were reduced by using the method mentioned above to get a new beam curve, named

as C-beam, from which the effect of Cyg A broadening has been removed. Then, the 3 dB and 10 dB beam-width of the C-beam in the two planes were measured. The antenna gain at this elevation position was then calculated by Equation (3),

$$G(\mathrm{dB}) = 10\lg\left[\frac{1}{2}\left(\frac{31000}{\theta_{3\mathrm{dBAz}}\times\theta_{3\mathrm{dBEl}}}+\frac{91000}{\theta_{10\mathrm{dBAz}}\times\theta_{10\mathrm{dBEl}}}\right)\right]-\Delta G_F-\Delta G_\sigma. \quad (3)$$

Table 7 and Figure 7 show the MRT50 gain variation with elevation at the S/X bands. There is a maximum in gain around elevation 25° at the S/X bands. This may be related to the MRT50 assembly procedure. The MRT50 maker made a reflector-shape adjustment at about elevation 30°. The gravitational change of the reflector-shape at X band may be smaller than that of the S band because the effective illuminating diameter of the MRT50 at S band is larger than that at X band. On the other hand, the outer part of the reflector may cause more gravitational shape-variation than the inner part does. This may be responsible for the obvious turn over in gain variation of S band in the low elevation region in the right panel of Figure 7.

Table 7 Measured Gains of MRT50 at S/X Bands

Gain at X band		Gain at S band	
Elevation (°)	Gain (dB)	Elevation (°)	Gain (dB)
11	69.48	10	58.85
15	69.46	15	58.78
20	69.61	20	58.77
25	69.53	25	59.11
30	69.41	30	58.80
35	69.43	35	58.85
40	69.33	40	58.95
45	69.35	45	59.08
50	69.31	50	58.78
55	69.25	55	58.70
60	69.22	60	58.62
65	69.21	65	58.81
70	69.17	70	58.57
75	69.18	74	58.56
80	69.20		

The method we used to measure the gain variation is not to determine the absolute amplitude of the gain at different elevations. We measure the beams in the two perpendicular planes at a series of elevations only so that the effect from atmosphereic attenuation on our measurements could be ignored. In addition, the observations were carried out during the dry and clear days, Sep. – Oct. 2007, the driest season in Beijing, so that atmospheric attenuation at X band may not be so serious. All of these may explain why the gain variations with elevation at X band and S band may not have a large difference.

5 EQUIVALENT NOISE TEMPERATURE AND ITS VARIATION

The system temperature of a radio telescope comes from receiver noise, background sky emission, ground emission, atmospheric emission and the antenna structure itself. Except for the receiver noise, the others vary with elevation of the antenna. This is also an important property to measure. The method we used is the same as that described in papers (Huang et al. 1988; Liu et al. 2002). In this paper, we take the LNA input-port as the reference point. A noise signal is injected at this point as the calibrator. All received noise power (within the same bandwidth) has been scaled to the temperature at this point. The measured results of system temperature variations are shown in Figure 8.

System temperature, the total noise temperature at the reference point, can be expressed as Equation (4) (Huang et al. 1984).

$$T_{\mathrm{sys}} = T_{\mathrm{r}} + (1-\eta)T_0 + \eta T_{\mathrm{sky},} \quad (4)$$

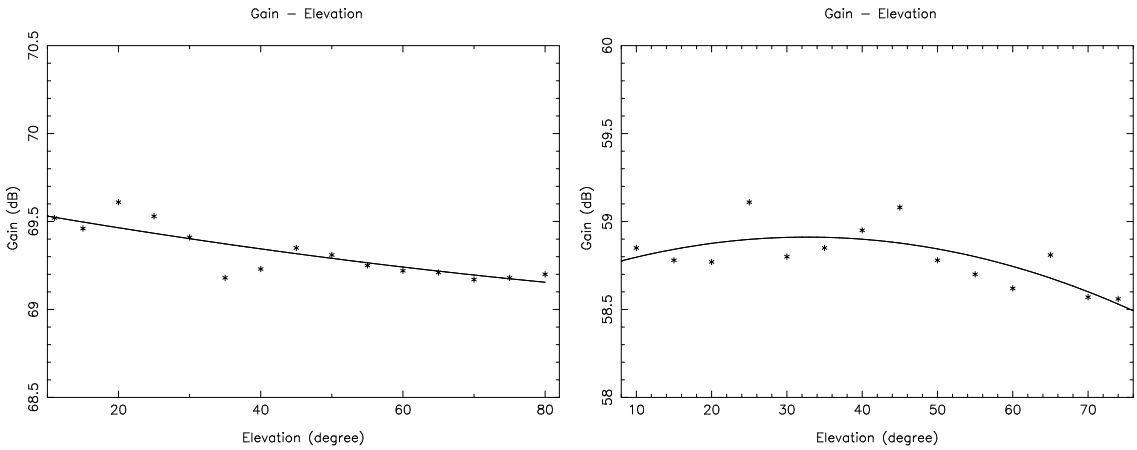

Fig. 7 Gain variations at X band (left) and S band (right).

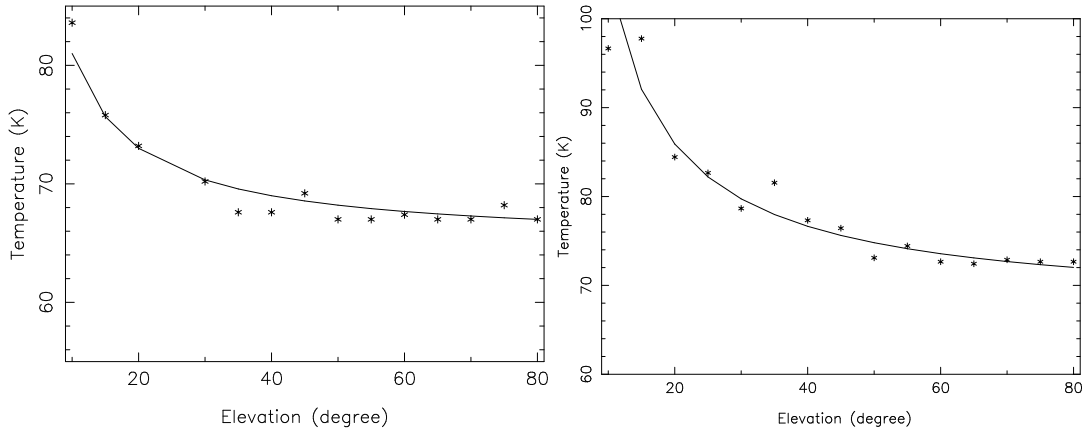

Fig. 8 X band (left) and S band (right) system temperatures of MRT50.

where T_0 is the ambient temperature, $T_{\rm sky}$ is the equivalent temperature contributed by the sky background emission, ground emission, atmospheric emission, and antenna structure at the feed output, $T_{\rm r}$ is the equivalent temperature of the receiver at the LNA input port, and η is the transmission efficiency between the feed output-port and the input-port of the LNA.

The Equation (4) can be re-written as $T_{\rm sys} = T_{\rm const.} + T_{\rm var.}$, where $T_{\rm const.}$ can be represented by the tangent-lines in the bottoms of Figures 10 and 11. The $T_{\rm r} + (1-\eta)T_0$ and the $T_{\rm sky}$ toward the zenith give the contribution to the $T_{\rm const.}$ from which we can estimate the transmission efficiency (η) between the feed output port and the input port of the LNA. Here, we give an example. For S band, the $T_{\rm const.}$ is about 72 K, $T_{\rm r}$ is about 20 K and T_0 is 291 K. The $T_{\rm sky}$ for the zenith direction can be estimated as follows (Anderson et al. 1991)

$$T_{\rm sky} = T_{\rm sky-bg}(\sim 2.7\,{\rm K}) + T_{\rm galac}(\sim 1\,{\rm K}) + T_{\rm atmos}(\sim 4\,{\rm K}) + T_{\rm spillover}(4 \sim 5\,{\rm K}) + T_{\rm scatter-support}(3-4\,{\rm K}) + T_{\rm leakage-mesh}(3-4\,{\rm K}). \quad (5)$$

Then we get $\eta_{\rm S} = 0.86 \pm 0.02$.

For X band, two main things are different. One is that the reflector for X band is the inner part of the whole reflector. Another is that the ratios of mesh surface to solid panel surface for X/S bands are 1.05 and 1.78 respectively. So both $T_{\rm spillover}$ and $T_{\rm leakage-mesh}$ at X band should be smaller than that at S band, whereas the $T_{\rm atmos}$ at X band is slightly larger than its value at S band. Taking these factors into account, we found $\eta_{\rm X} = 0.90 \pm 0.02$.

6 SUMMARY

The main points of this paper are listed as follows.

(1) Pointing accuracy of the MRT50 (rms) is 13.5″ in the azimuth direction and 17.5″ in the elevation directions, respectively.
(2) Measured the two-dimensional main beams at S/X bands. The main beam efficiency is 87.4% and 84.8% at S/X bands respectively. The beams show a symmetric shape.
(3) Measured gains and its variation with elevation at S/X bands. No large gain variations with elevation from 10°– 80° elevation were found, although the trends of S/X band show some differences. The tune-over of S band gain variation in the low elevation region may be caused mainly by the outer part of the reflector.
(4) Measured system temperature and its variation with elevation at S/X bands. The system temperature varies from 62 – 76 K and 72 – 100 K at X/S bands for elevation 80° –10° and gets the estimated transmission efficiencies between the feed output port and the input port of the LNA at S/X bands, which is $\eta_{\rm S} = 0.86 \pm 0.02$ and $\eta_{\rm X} = 0.90 \pm 0.02$ respectively.
(5) Developed a new program to remove the broadening effect on beam measurement when using an extended source as the emitting source.

Acknowledgements Authors thank Prof. Liang Shiguang for the long-term cooperation in radio astronomy and especially for the preparation of the new radiometer and thank Mr. Cao Xiandong for his helps with the sampling program development. We are also thankful to the MRT50 operators for their assistance during all the observations.

References

Anderson, M. D., Routedge, D. V., Vaneldik, J. F., & Landecker, T. L. 1991, Radio Science, 26, 353
Himwich, W. E. 1993, Pointing Model Derivation, Operation Manual of VLBI Mark IV Field System
Huang, X. Y., & Gao, Y. H. 1991, Annals of Shanghai Observatory Academia Sinica, 12, 127
Huang, Y. R., Xu, A. A., Tang, Y. H., et al. 1984, Observational Astrophysics, 483 (in Chinese)
Isber, A. M. 1967, Microwaves, August, 40
Jin, C., Cao, Y., Chen, H., et al. 2006, ChJAA (Chin. J. Astron. Astrophys.), 6S2, 319
Johannsen, K. G., & Titus, L. 1986, IEEE ON IM, IM-35, 344
Kong, D. Q., Shi, H. L., Zhang, X. Z., & Zhang, H. B. 2008, Journal of Xidian University, 35, 157
Liu, X. 2002, Technique Report of the Urumiq Astronomical Observatory, 134
Meeks, M. L., Ball, J. A., & Hull, A. B. 1968, IEEE Trans. ON AP, AP-16, 746
Stutzman, W. L. 1998, IEEE Trans. On AP, AP-40, 7
Ulich, B. L. 1981, International Journal of Infrared and Millimeter Waves, 2, 293
Ulich, B. L. 1982, SPIE, 332, 33
Wang, S. G., Zhu, Z. H., Zhou Z. L., & Zhang, Y. Z. 2002, IJMPD, 11, 1061
Yuan, H. R., Peng, Y. L., & Xue, Y. Z. 1986, Antenna Parameter Measurement Using Radio Astronomical Technique, Electronic and Industry Press, 147 (in Chinese)
Zhang, X. Z., et al. 2000, in Proceedings of Kanasi Pulsar Observation and Research Meeting, ed. Zhang J., 139
Zhang, J. Y. 2007, PhD Thesis, 2007, 101
Zhang, X. Z., Zheng, Y. J., Chen, H. S., et al. 1997, A&AS, 121, 59
Zhang, X. Z. 2007, ChJAA (Chin. J. Astron. Astrophys.), 7, 712